Available online at www.sciencedirect.com
ScienceDirect
Trans. Nonferrous Met. Soc. China 35(2025) 2449−2461
Transactions of Nonferrous Metals Society of China
www.tnmsc.cn

Aging behavior, microstructure and mechanical properties of graphene nanosheets reinforced A380 composites

Zhao-wei HUANG[1,2], Xiao-bin LU[3], Hong YAN[1,2]

1. School of Advanced Manufacturing, Nanchang University, Nanchang 330031, China;
2. Key Laboratory of Light Alloy Preparation & Processing in Nanchang City, Nanchang 330031, China;
3. Luxe Machinery (Gaoan) Co., Ltd., Gaoan 330800, China

Received 27 November 2023; accepted 19 July 2024

Abstract: Graphene nanoplatelets (GNPs) reinforced A380 composites (GNPs/A380 composites) were prepared by ultrasonic vibration casting method. The microstructure, aging behavior and mechanical properties of the composites were investigated. It was found that the peak aging time of GNPs/A380 composites could be decreased by GNPs. The GNPs−Al interface could serve as a more stable nucleation site for the precipitated phases. With bridging GNPs, the coordinated deformation of the matrix is increased and larger dimples appear on the fracture surface of GNPs/A380 composites. The yield strength of the GNPs/A380 composites increased by 28.1% compared with that of the A380 alloy due to the fine grain strengthening, load transfer and precipitation strengthening mechanisms.

Key words: graphene nanoplatelet; aluminum matrix composite; aging treatment; microstructure; mechanical properties

1 Introduction

Carbon nanomaterials are considered the most promising reinforcing materials for aluminum matrix composites due to their extraordinarily high elastic modulus and mechanical strength, as well as excellent thermal conductivity [1−3]. The introduction of carbon nanomaterials can effectively improve the specific strength and specific modulus of aluminum matrix composites [4]. Among the many carbon nanomaterials, graphene nanoplatelets (GNPs) have received more attention due to their high specific elastic modulus, specific surface area, and unique thermal properties [5]. Many studies have shown that reinforcing aluminum matrix composites with GNPs can effectively improve the properties of the composites [6,7]. Due to fine grain strengthening, Orowan strengthening, load transfer strengthening and thermal mismatch strengthening mechanisms, the mechanical properties of aluminum alloy composites can be significantly enhanced by GNPs [8]. Depending on the preparation process and GNPs content, the properties of the composites can be improved to a high or low level. Most previous studies have focused on improving the dispersion of GNPs. With the advent of technologies such as high-energy ball milling [9,10], wet mixing [11,12], and sheet powder metallurgy [13,14], the problem of graphene dispersion in composites has been well solved. YU et al [15] prepared GNSs/Al6063 composites by pressure infiltration method and investigated the interfacial reaction between GNSs and Al matrix. The results showed that ball milling damaged the structure of graphene, leading to an increase in the interfacial product of Al_4C_3 phase, which destroyed the integrity of GNSs and limited

Corresponding author: Hong YAN, Tel: +86-791-83969622, E-mail: hyan@ncu.edu.cn
https://doi.org/10.1016/S1003-6326(25)66826-9

the enhancement effect of GNSs. LI et al [16] used a novel two-part method to prepare GNPs/Al composites. The Al_4C_3 phase in the composites was significantly reduced by using magnetic stirring plus short-time ball milling instead of long-time ball milling. Hence, the protection of the GNPs' structure should be considered when dispersing the GNPs.

In recent years, GNPs−Al interface bonding has been widely investigated as a hot topic in the study of GNPs reinforced aluminum matrix composites [17,18]. However, there are few studies on the aging behavior of GNPs. Among the commercially available Al−Si−Cu casting alloys, A380 alloy is the most commonly used alloy for cylinder heads and engine blocks. The intermetallic β-Al_5FeSi phase formed during the solidification of A380 alloys is long and needle-like, and the eutectic Si phase is also relatively coarse. The tip regions of these brittle phases tend to stress concentrations and promote cracking [19]. The transformation of the second phase can be achieved using heat treatment, and the precipitated phase during aging can also enhance the strength of A380 alloys [20]. The aging behavior of the reinforcing phase during aging treatment is complex [21−26]. The aging behavior of reinforced aluminum matrix composites differs depending on the matrix alloy, the reinforcement and the preparation process.

The aging enhancement effect is enhanced when using TiC reinforced aluminum matrix composites, due to the increased dislocation density of TiC, which promotes the precipitation process [22]. In the case of carbon nanotube (CNT) reinforced 6061 Al composites, the addition of CNT leads to an indirect depletion of the Mg element, resulting in a reduction of Mg_2Si precipitates, which counteracts the great benefit of CNT [23]. The vacancy concentration of SiC/Al−Cu−Mg composites is reduced by the addition of SiC, resulting in longer peak aging time than in Al−Cu−Mg alloys [24].

The corrosion resistance is decreased by 39% after aging treatment for in-situ generation of aluminized nickel reinforced Al−Zn−Mg−Cu alloy composites [25]. The maximum hardness and ultimate tensile strength of AA2024−Al3NiCu composites are reduced by 6% and 4%, respectively, compared with the nickel-free AA2024 Al alloy [26].

As can be seen, the aging behavior of aluminum matrix composites is an important and challenging area of research. However, as far as we know, the effect of GNPs on the aging behavior of GNPs/A380 composites has been rarely reported.

In this work, as-cast GNPs/A380 composites were prepared. The changes in microstructure morphology and mechanical properties after aging were characterized. The effect of microstructural changes induced by GNPs on the aging of GNPs/A380 composites was investigated. The microstructural changes at the GNPs−Al interface during aging treatment were characterized, and the strengthening mechanisms and effects of GNPs/A380 composites were analyzed. This work has provided a new guide for developing high-performance GNPs/Al composites.

2 Experimental

2.1 Preparation of composites

According to our previous research [27], the as-cast GNPs/A380 composites prepared using ultrasonic vibration exhibit the best performance when the GNPs addition is 1.0 wt.%. Hence, 1.0wt.%GNPs/A380 composites were selected to further study the effect of aging treatment on GNPs/A380 composites. The chemical composition of the A380 alloys and the parameters of the GNPs are shown in Tables 1 and 2, respectively. The GNPs were produced by the Chinese Academy of Sciences, Chengdu Organic Chemistry Co,.

Table 1 Chemical composition of A380 alloys (at.%)

Si	Cu	Fe	Mg	Mn	Zn	Ti	Al
10.22	2.00	1.51	0.20	0.13	0.10	0.04	Bal.

Table 2 Performance parameters of multilayer graphene nanoplatelets

Purity/ wt.%	Layer number	Thickness/ nm	Diameter/ μm	Density/ ($g·cm^{-3}$)
>99.5	<20	≤10	≤10	0.6

The GNPs/A380 composites were prepared in three steps as shown in Fig. 1. The first step is described as follows: First, GNPs were added to the ethanol solution and sonicated in an ultrasonic cleaner for 1 h with an ultrasonic power of 120 W. Simultaneously, pure Al powders (particle size

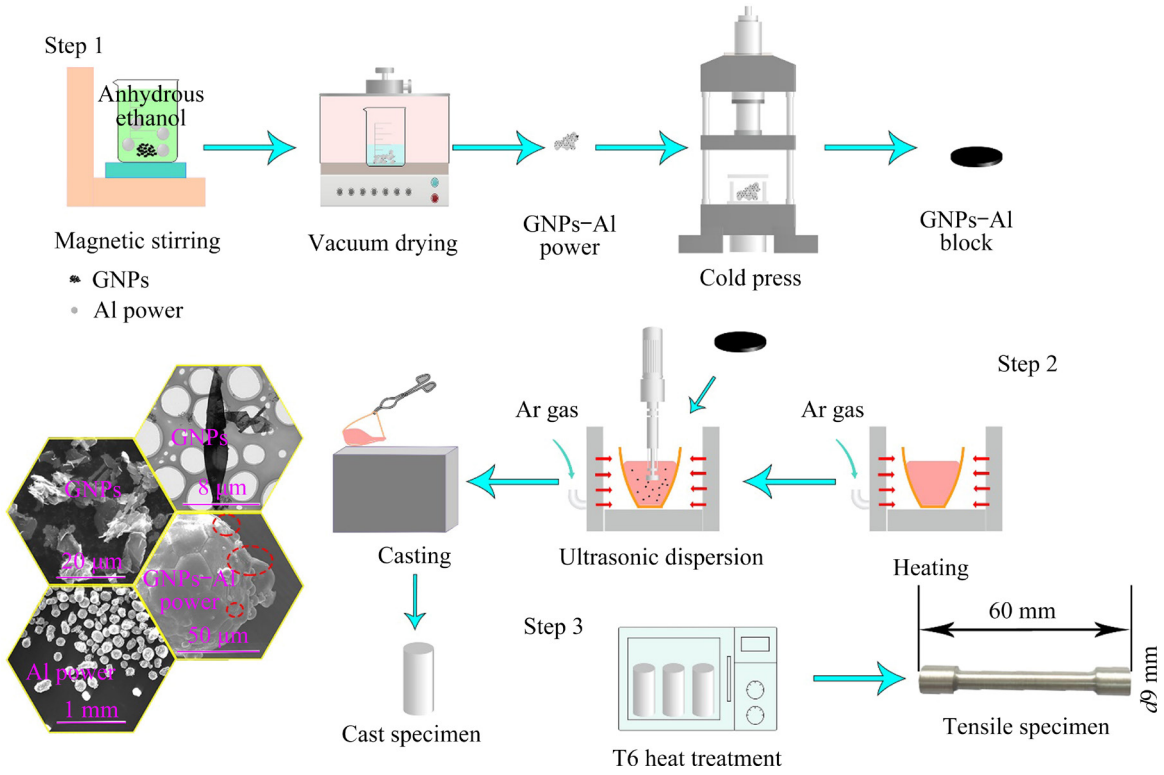

Fig. 1 Original material morphology and schematic diagram of fabricated composites

<300 μm, purity ≥99%) were added to the ethanol solution and mixed by mechanical stirring at a speed of 120 r/min for 1 h. Next, the GNPs/ethanol solution was added to the Al powder/ethanol solution, and the mixed solution continued to undergo ultrasonication for 1 h with an ultrasonic power of 120 W. After the ultrasonic dispersion treatment, the mixed solution was transferred to a magnetic stirrer and magnetically stirred for 2 h at a speed of 1200 r/min and a temperature of 60 °C. Then, the mixed slurry was placed into a vacuum drying oven and dried at 80 °C for 12 h to obtain GNPs−Al powders. Lastly, the GNPs−Al powders were cold-pressed using a stainless-steel mold under a pressure of 60 MPa to obtain the GNP−Al prefabricated blocks. The GNPs−Al prefabricated blocks were cylinders with a diameter of 3.5 cm, which contained 10 wt.% GNPs.

The second step involved the fabrication of cast GNPs/A380 composites. Firstly, the A380 alloys were placed in an Al oxide crucible, heated to 780 °C in a resistance furnace, and held for 30 min. After the alloy was completely melted, slagging was performed using hexafluoroethane (HFO). Then, an intermediate alloy block of GNPs−Al covered with Al foil was added to the molten mixture. Meanwhile, ultrasonic vibrations were applied using an ultrasonic metal welder (with an ultrasonic frequency of 20 kHz, ultrasonic power of 2.8 kW, and ultrasonic time of 12 min). Finally, the melt was poured into a dry stainless-steel mold. For comparison, cast A380 alloys were fabricated under the same conditions. Throughout the experiment, the melt was protected with argon gas.

The third step involved heat treatment of the as-cast GNPs/A380 composites and the as-cast A380 alloys. For the A380 samples, a short solid solution treatment time (2 h) at 515 °C was enough to transform the β-Al5FeSi phase into the α-Al_8Fe_2Si phase [28]. The GNPs/A380 composites and A380 alloys were solution treated at 515 °C for 2 h and then quenched in water at 25 °C. Finally, they were aged at 155 °C. The hardness of the samples was measured every 2 h.

2.2 Tensile and hardness test

The size of the dog-bone tensile specimens was d9 mm × 60 mm. The tensile test was performed using a WDW−200GD tensile tester at a strain rate of 0.001 s^{-1}. The Vickers hardness was measured on an HVS−1000A hardness tester applying a load of 100 g for 10 s.

2.3 Material characterization

The morphology of the GNPs was observed using both field emission scanning electron microscopy (SEM, Quanta 200F) and transmission electron microscopy (TEM, JEM−2100). The microstructure of as-cast A380 alloys and GNPs/A380 composites was observed utilizing the same SEM equipment. The microstructures of the peak-aged A380 alloys and GNPs/A380 composites were investigated using an optical microscope (OM, Nican-M300). The fracture surface of samples was investigated using the same SEM equipment. The phases were analyzed by X-ray diffraction (XRD−600). The microstructure of the GNPs/A380 composite was observed using the same TEM equipment.

3 Results and discussion

3.1 Microstructure

SEM images and EDS results of A380 alloys and GNPs/A380 composites are shown in Fig. 2. It can be seen that A380 alloys mainly consist of α-Al, coarse Si phase, and long needle-like β-Al_5FeSi phase. The EDS results show that there is no significant agglomeration of the GNPs, as shown in Fig. 2(b). Due to poor electrical conductivity, the Si phase is not as obvious as the other phases in the SEM image. But from the EDS results, it can be seen that the sizes of the coarse Si phase and the long needle-like β-Al_5FeSi phase decrease. Additionally, the microstructure after peak aging was observed using OM, as shown in Fig. 3. Figure 4 shows the XRD patterns of A380 alloys and GNPs/A380 composites after peak aging. As can be seen from Fig. 4, both A380 alloys and GNPs/A380 composites contain the α-Al_8Fe_2Si phase. This mainly occurs during the material solution treatment process of β-Al_5FeSi phase transformation [28]. During the solution treatment, Al_2Cu was dissolved into the matrix and precipitated during aging treatment [29,30]. Due to the limitation of the magnification of OM, the Al_2Cu phase is not observed in Fig. 3, but it is detected in Fig. 4. As can be seen from Fig. 3, after peak aging, the Si phase undergoes transformation to a rounded shape. The microstructure of the GNPs/A380 composites is not much different from that of the A380 alloys under OM observation.

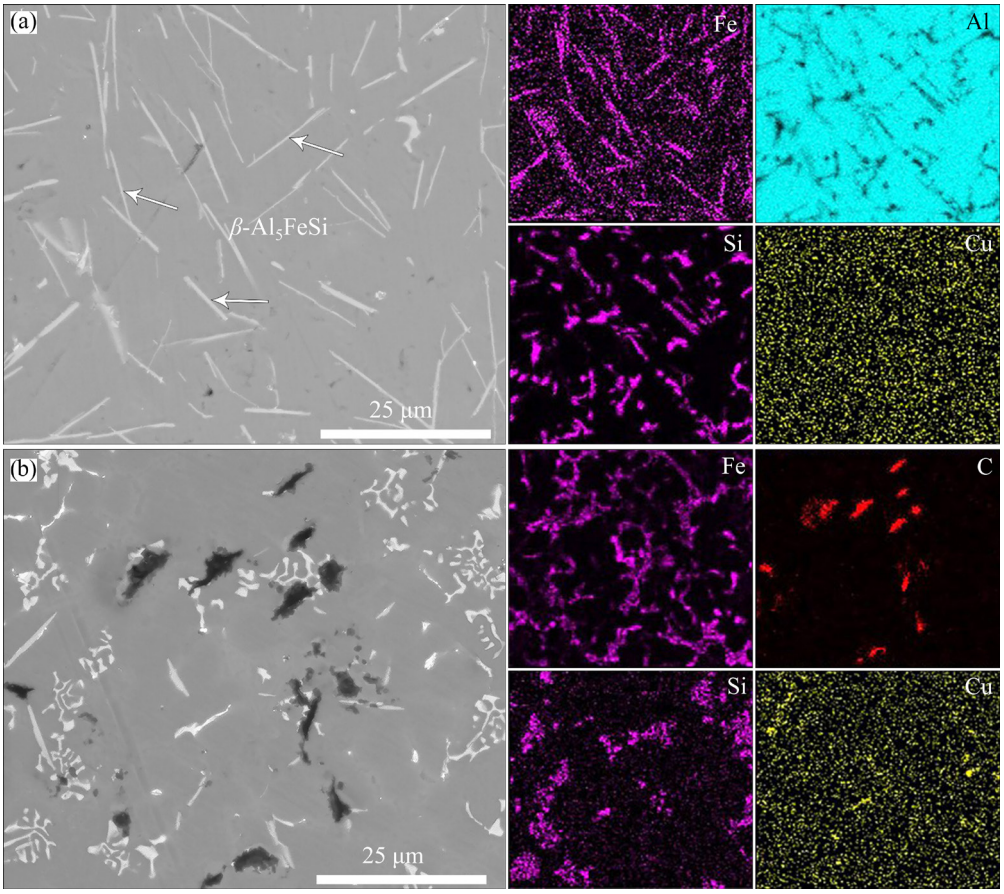

Fig. 2 SEM images and EDS results of A380 alloys (a) and GNPs/A380 composites (b)

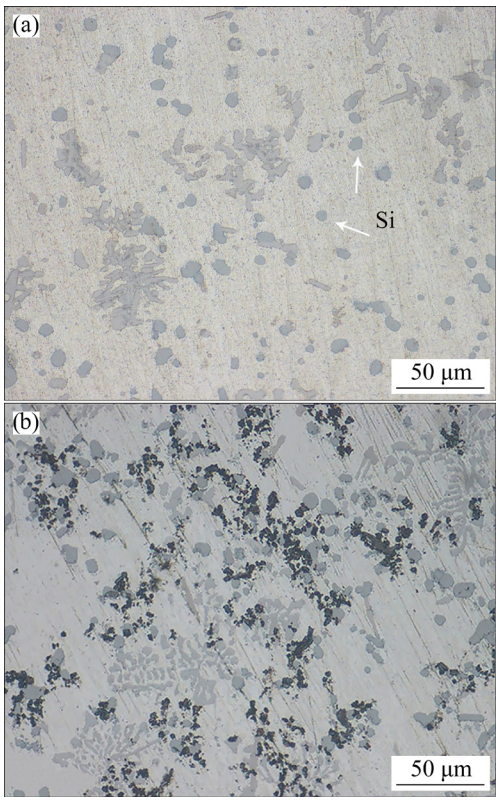

Fig. 3 OM images of peak-aged A380 alloys (a) and peak-aged GNPs/A380 composites (b)

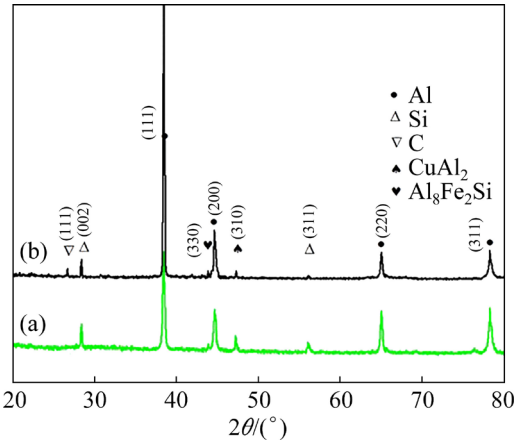

Fig. 4 XRD patterns of peak-aged A380 alloys (a) and peak-aged GNPs/A380composites (b)

3.2 Hardness properties of composites

The hardness test results of the A380 alloys and GNPs/A380 composites aged at 155 °C are displayed in Fig. 5. It can be seen that the hardness of A380 alloys increases with the increase of aging time and then reaches a peak value. However, with the further increase of aging time, the hardness of A380 alloy significantly decreases. This phenomenon is attributed to the precipitation of Cu element during aging treatment. Cu element precipitates out of the Al matrix according to the sequence of GP zone → θ'' phase → θ' phase → θ phase (Al_2Cu) [31]. The strain field near the precipitated phase increases and then decreases. Meanwhile, the hardness of the alloy shows a pattern of increasing and then decreasing. A similar trend is observed in GNPs/A380 composites. When aging for 8 h, the hardness of GNPs/A380 composites reached a peak of HV 168.4. Clearly, the peak aging time of GNPs/A380 composites is shorter than that of A380 alloy.

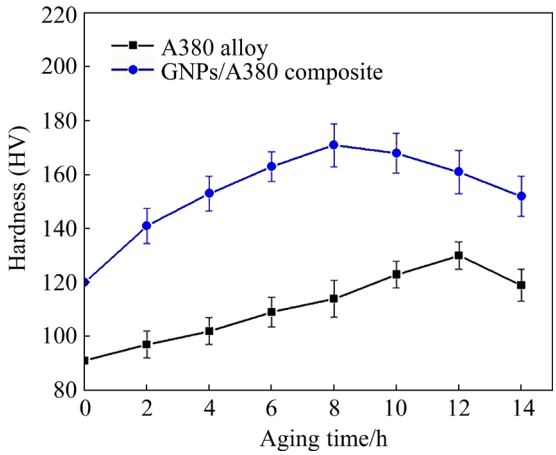

Fig. 5 Hardness curves of A380 alloys and GNPs/A380 composites aged at 155 °C for different time

3.3 TEM analysis results

When the aging treatment was 2 h, the hardness of the GNPs/A380 composites showed a significant increase. The microstructure of GNPs/A380 composites was observed using TEM to investigate the effect of GNPs on aging treatment. Figure 6 shows the microstructure of the 2 h aging treatment of the GNPs/A380 composites. Several flaky phases can be seen in Fig. 6, and the selected area electron diffraction (SAED) result is shown in Region I. These flake phases can be identified as added GNPs. A large number of dislocations can be seen in Region II. Due to the large difference in coefficients of thermal expansion (CTE, μ) between GNPs and Al matrix, a large number of geometrically necessary dislocations were generated after solid solution treatment. The magnified image of Region II showed a large number of precipitated phases. The magnified image of Region III showed that these precipitated phases nucleated and grew in the vicinity of the dislocations. This indicates that the precipitated

phase is responsible for the significant increase in hardness of the material.

Figure 7 shows the microstructure of the peak-aged GNPs/A380 composites. The distribution of elements in Fig. 7(a) is shown in Figs. 7(b−e). Figure 7(a) shows that the distribution of the lamellar GNPs corresponds exactly to the distribution of the C element. Due to the interfacial reaction between GNPs and the Al matrix, the brittle Al_4C_3 phase was often observed at the GNPs/Al interface. CHEN et al [32] noted that the Al_4C_3 phase often occurred at structural defects in GNPs. HRTEM shows that slight elemental diffusion occurs between GNPs and Al, as shown in Fig. 7(g). The GNPs are observed in magnification as shown in Figs. 7(f, g). It is observed that the GNPs form a very clean contact with the aluminum matrix and no brittle Al_4C_3 phase is observed. The disappearance of the Al_4C_3 phase is due to two reasons. One is the use of lower energy magnetic stirring rather than ball milling, which protects the microstructural integrity of the GNPs. The other is

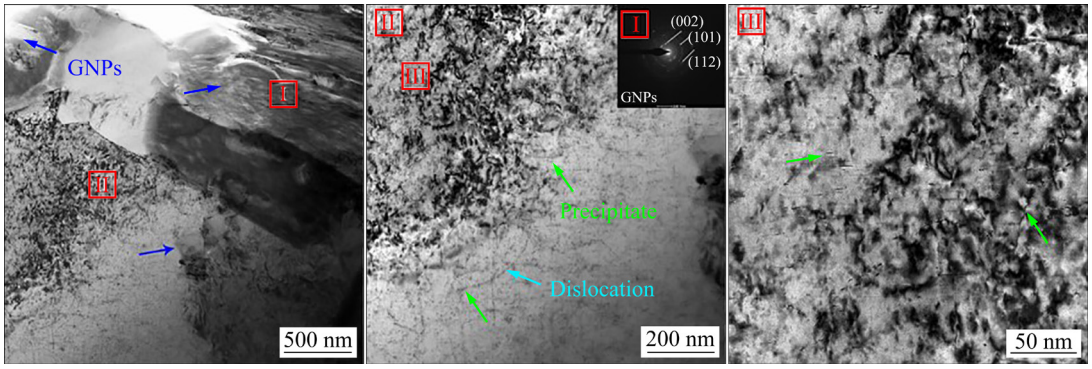

Fig. 6 TEM image of GNPs/A380 composites after aging for 2 h

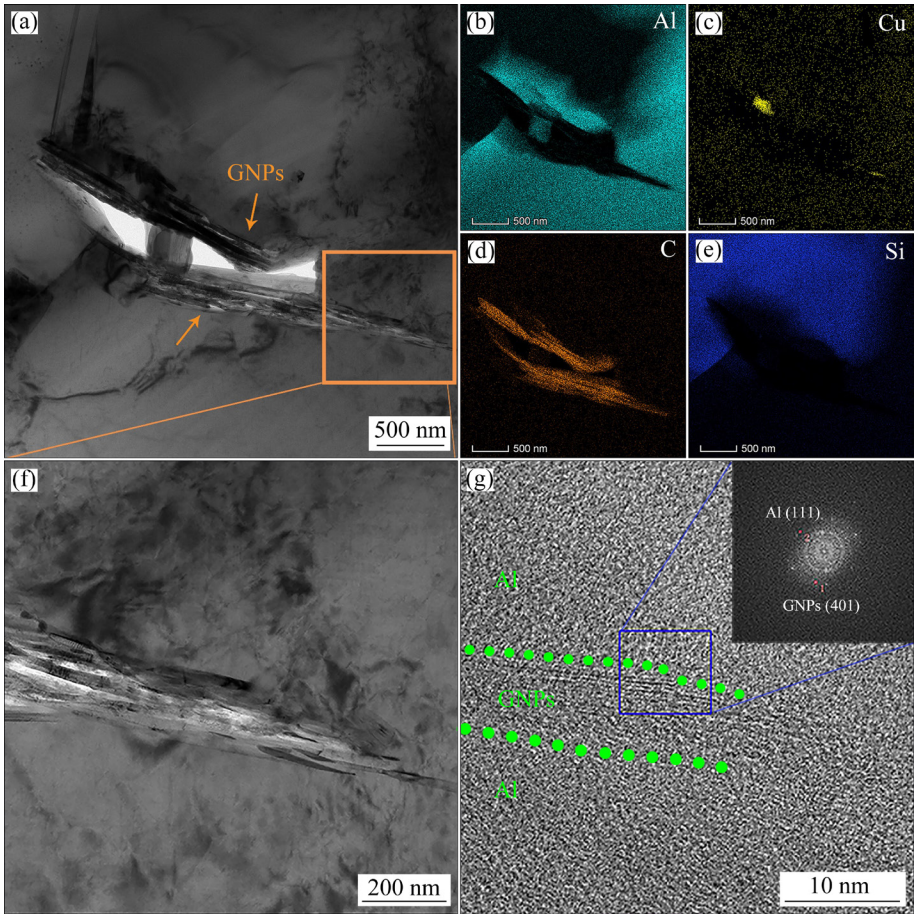

Fig. 7 TEM images of peak-aged GNPs/A380 composites: (a) Microstructure of GNPs; (b−e) EDS results corresponding to (a); (f) Magnification of corresponding area in (a); (g) HRTEM image of GNPs−Al interface

the use of ultrasonic vibrations during the preparation of the GNPs/A380 composites. When the reaction temperature exceeds 2728 K, the reaction ($4Al+3C \rightarrow Al_4C_3$) will be inhibited [33]. When ultrasonic vibrations were applied to the melt, the instantaneous temperature could reach 1×10^4 K, which could inhibit the formation of the Al_4C_3 phase [34]. Only a few dislocations are found in the Al matrix, which indicates that a large number of dislocations have been annihilated or rearranged after the 8 h aging treatment.

As can be seen from Fig. 7(c), the Cu element appears to be significantly polarized. Compared with the Al matrix, Cu element is more inclined to be enriched at the GNPs−Al interface. To investigate the effect of the GNPs−Al interface on the precipitated phase, the GNPs−Al interface was observed under HAADF mode, as shown in Figs. 8 and 9, respectively. Figure 8 shows the TEM image of the GNPs/A380 composites aged for 6 h.

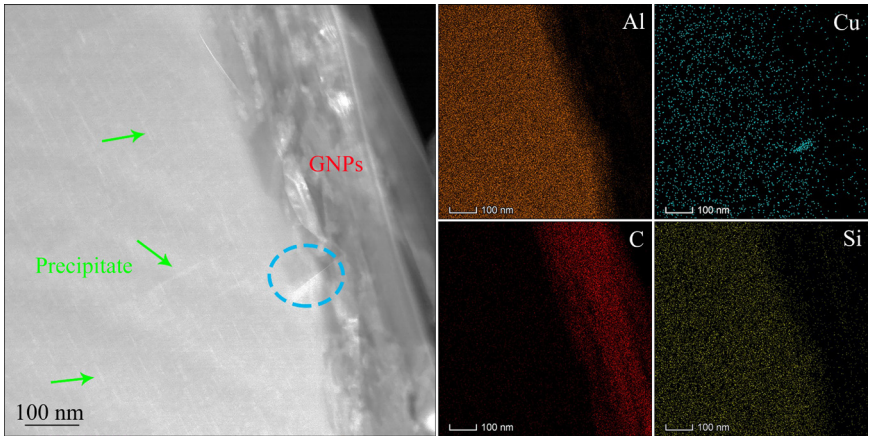

Fig. 8 HAADF-TEM image and EDS results of GNPs/A380 composites after aging for 6 h

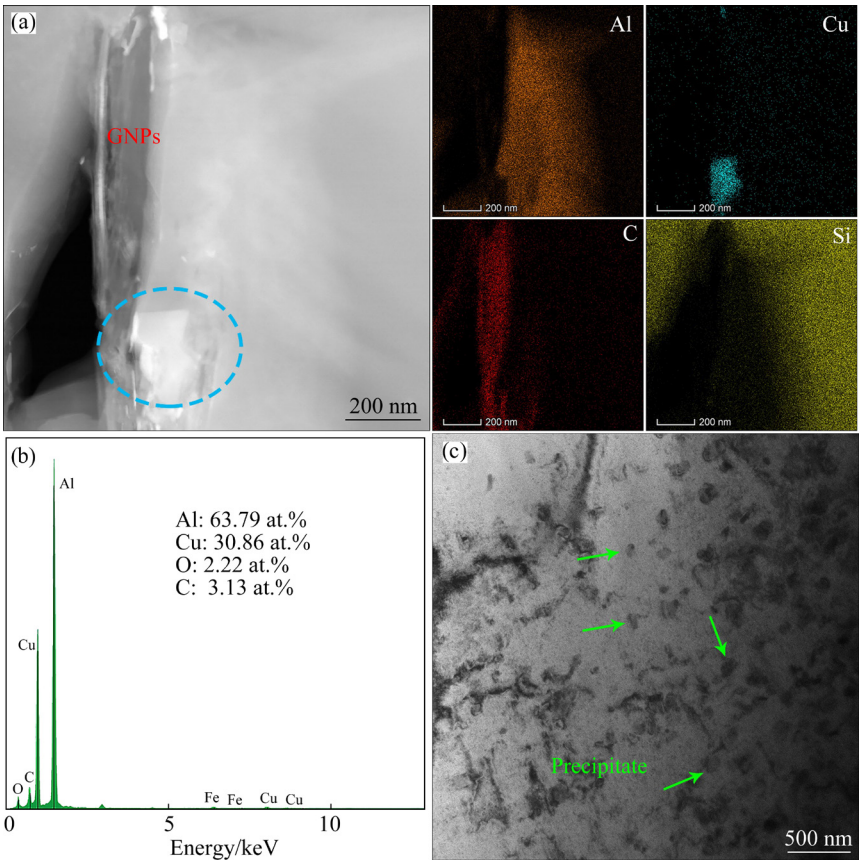

Fig. 9 TEM image of GNPs/A380 composites after aging for 10 h: (a) HAADF-TEM image and corresponding element maps; (b) EDS results for corresponding blue cross in (a); (c) Microstructure of precipitated phase in Al matrix

The typical precipitated θ' phase with a size of around 100 nm was observed in the Al matrix. Due to the small size and uniform distribution of the precipitated phase, no enrichment of Cu element was observed in the Al matrix. On the contrary, the enrichment of Cu element occurred at the GNPs−Al interface. Different from the θ' phase, the Cu element-enriched phase was irregularly blocky.

Figure 9 shows the TEM image of the GNPs/A380 composites aged for 10 h. From Fig. 9(c), it can be seen that the precipitated phase in the Al matrix changes to a granular shape with a size of around 120 nm. Due to the long aging treatment, the precipitated θ' phase transformed into an equilibrium precipitated Al_2Cu phase. The strain field around the precipitated phase is weakened when the precipitated phase is completely disengaged from the matrix. As a result, the hardness of the GNPs/A380 composites showed a decrease during the aging treatment for 10 h. As can be seen from Fig. 9(a), the enrichment of Cu element also appeared at the GNPs−Al interface. Figure 9(b) shows the EDS results for the corresponding blue cross in Fig. 9(a). The results show that the atomic ratio of Al to Cu is about 2:1, which is in close agreement with the Al_2Cu phase. The size of the Cu-enriched phase is significantly larger than that of the precipitated phase in the Al matrix, with a size of about 200 nm. This indicates that more Cu elements are enriched at the GNPs−Al interface during aging. This can be explained by the decrease in dislocation density due to dislocation annihilation during the aging treatment, which causes a decrease in the atomic diffusion rate, while the GNPs−Al interface is not affected. In other words, the GNPs−Al interface can act as a more stable and faster atomic diffusion channel during the aging treatment.

3.4 Tensile properties and strengthening mechanism of composites

Figure 10 shows the mechanical properties of the two materials at peak aging. The yield strength, ultimate tensile strength and elongation of peak-aged A380 alloys are 174 MPa, 247.3 MPa, and 3.5%, respectively. The tensile properties of the GNPs/A380 composites are significantly improved after aging treatment. The yield strength and ultimate tensile strength (223 MPa, 308.7 MPa) are increased by 49 MPa and 61.4 MPa respectively. The longer aging time of the A380 alloys allowed grain growth to offset part of the precipitation strengthening. The shorter peak aging time and the inhibition of grain growth by GNPs resulted in more significant precipitation strengthening of the GNPs/A380 composites.

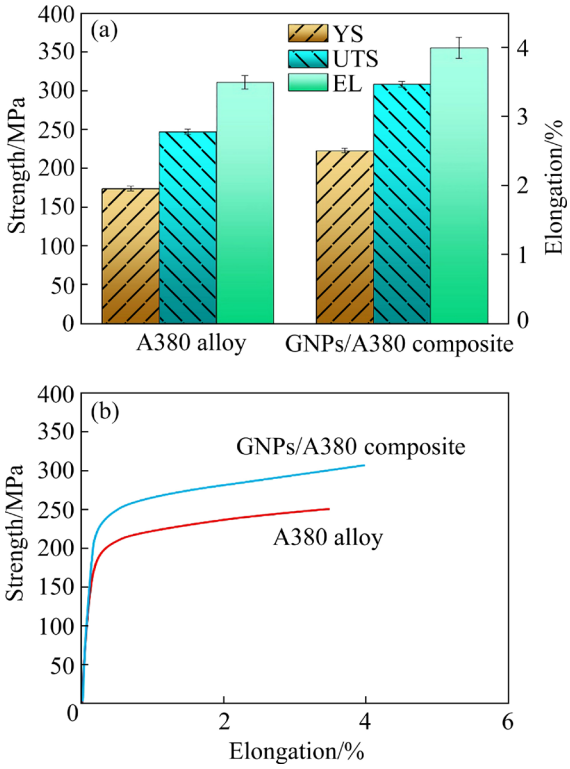

Fig. 10 Mechanical properties of peak-aged A380 alloy and GNPs/A380 composite

Several strengthening mechanisms, such as grain refinement, load transfer, and thermal mismatch mechanisms, are often used to discuss GNPs for strengthening metal matrix composites. The effectiveness of each strengthening mechanism depends on the microstructure. The Orowan mechanism is more applicable to nanoceramic materials [35] and therefore the contribution is neglected. LI et al [36] pointed out that the significant strengthening effect of CTE in GNP/Al composites is not applicable after heat treatment. This may be due to the release of residual stresses during aging and the two-dimensional flexible structure of the GNPs. It is also noted from the above that the dislocations due to CTE are largely obliterated after the aging process. The content of Cu element is constant, but the addition of GNPs also affects the distribution and size of the

precipitation phase, which leads to difference in precipitation enhancement ($\Delta\sigma_{ps}$). Using well-accepted rules for mixing models, the yield strengthening (σ_c) of GNPs on GNPs/A380 composites can be expressed as

$$\sigma_c=\Delta\sigma_{GR}+\Delta\sigma_{LT}+\Delta\sigma_m(1-v) \quad (1)$$

where $\Delta\sigma_{GR}$ and $\Delta\sigma_{LT}$ are the contributions to the yield strength of the composites provided from the refinement strengthening and load transfer strengthening, respectively, σ_m is the yield strength of peak-aged A380 alloy, and v is the volume fraction of GNPs.

By hindering grain growth, GNPs can refine grains. Finer grains mean that there are more grain boundaries to impede the movement of dislocations. In this work, α-Al is a dendritic crystal, so the grain size is calculated using the equivalent diameter. The contribution of grain refinement to strength can be calculated according to the Hall−Petch equation [37]:

$$\Delta\sigma_{GR}=K(d_{com}^{-1/2}-d_{alloy}^{-1/2}) \quad (2)$$

where K is the Hall−Petch coefficient, d_{com} and d_{alloy} are the average grain sizes of GNPs/A380 composites and A380 alloys, respectively. The calculated $\Delta\sigma_{GR}$ is about 11.8 MPa.

The maximum load transfer effect of GNPs can be predicted using the Kellye−Tyson equations [38]:

$$\Delta\sigma_{LT}^{Max}=S\tau v \quad (3)$$

where S is the aspect ratio of GNPs, and τ is the shear stress of GNPs−Al interface. Thus, the $\Delta\sigma_{LT}$ for peak-aged GNPs/A380 composites is calculated to be about 31.3 MPa. Knowing the values of $\Delta\sigma_{GR}$ and $\Delta\sigma_{LT}$, $\Delta\sigma_{ps}$ can be calculated as

$$\Delta\sigma_{ps}=\Delta\sigma_c-(\sigma_m+\Delta\sigma_{GR}+\Delta\sigma_{LT})(1-v) \quad (4)$$

Thus, the addition of GNPs resulted in increase of 9.2 MPa in $\Delta\sigma_{ps}$.

3.5 Mechanism of accelerated aging

The diffusion of the Cu element and the nucleation of the Al_2Cu phase directly affect the precipitation of the Al_2Cu phase during the aging process. The GNPs/A380 composites have a much shorter peak aging time, and undoubtedly, the GNPs are critical. Hence, the effect of GNPs on the diffusion of Cu element and the nucleation of Al_2Cu deserves to be discussed in detail.

The interface between GNPs and Al is an incoherent interface and GNPs do not increase the nucleation sites of Al [39]. However, by hindering grain growth [40], GNPs refine grain size and lead to more grain boundaries. During aging, defects at grain boundaries, phase interfaces, and dislocations become preferential nucleation sites for the precipitated phase [41]. The addition of GNPs resulted in a large number of GNPs−Al interfaces appearing. Therefore, the precipitation of the Al_2Cu phase will be accelerated with the help of the phase interface. Moreover, the precipitation rate of Al_2Cu phase at the GNPs−Al interface is faster than that in the Al matrix.

During aging, the GNPs at the grain boundaries hinder the growth of the grain. Hence, the size of the grain changes little after aging. A large number of grain boundaries can reduce the non-uniform nucleation activation energy (D) of the precipitated phase [42,43], according to the Arrhenius equation [41]:

$$D=D_0\exp\left(-\frac{Q}{RT}\right) \quad (5)$$

where D_0 is the diffusion constant, Q is the activation energy, R is the molar gas constant, and T is the thermodynamic temperature. Clearly, the rate of diffusion is inversely proportional to the activation energy. Therefore, the addition of GNPs leads to the appearance of more grain boundaries and can promote Al_2Cu phase precipitation.

Due to the large difference in thermal coefficients between GNPs and the Al matrix, a large number of dislocations are created around the GNPs to balance the stresses caused by the CTE difference. The dislocation density (ρ) is shown as [44]

$$\rho=Bf_{GNP}\Delta\mu\Delta T/bt(1-f_{GNP}) \quad (6)$$

where B is the geometric constant, t is the dimension of GNPs, f_{GNP} is the volume fraction of GNPs, $\Delta\mu$ is the difference in coefficient of thermal expansion, ΔT is the difference between processing and testing temperature, and b is the magnitude of Burgers vector.

The dislocation density of the GNPs/A380 composites after solid solution treatment is calculated to be about 2.7×10^{14} m^{-2}. For annealed metals, the dislocation density is typically 1×10^{10}–

1×10^{11} m^{-2} [41]. Therefore, the addition of GNPs increases the high density of dislocations. In general, GNPs promote the nucleation and growth to reduce the peak aging time during aging treatment.

The precipitated Al_2Cu phase generates an elastic strain field in the Al matrix, inhibiting the movement of dislocations. The contribution of the relative strength of Al_2Cu can be calculated by the following equation [45].

$$\Delta\sigma_{or}=M\frac{0.4Gb}{\pi\sqrt{1-\upsilon}}\frac{\ln(2r/b)}{\lambda} \quad (7)$$

where M is the Taylor coefficient (3.06), G is the shear modulus (Al ~25.4 GPa), υ is the Poisson's ratio (Al ~0.35), r is the mean precipitate radius, and λ is the spacing between mean precipitates. When the volume fraction of the precipitated phase is constant, a smaller average radius has a better reinforcement effect.

3.6 Toughening of graphene

Normally, an increase in the tensile strength of composites is often achieved at the expense of plasticity [46]. It is noted that the elongation of the GNPs/A380 composites is high. Hence, the tensile fracture surface is observed, as shown in Fig. 11. Shallow dimples and tear ridges can be seen on the fracture surface of the peak-aged A380 alloy, as shown in Fig. 11(a). The reason for the dimples is the fact that the second phase is less deformable than the Al matrix. Under stress, the second phase deforms. However, the coordinated deformation of the second phase is limited and the stress cannot be fully released. Therefore, the second phase breaks down, causing fracture and the formation of fine micro-pores, i.e. dimples [47]. The fracture surfaces of the peak-aged GNPs/A380 composites are shown in Figs. 11(b, c). Many tiny dimples and several large dimples with wrinkle-like phases are seen in Fig. 11(b). The folded phases are identified as GNPs based on the EDS results of the rectangular area in Fig. 11(d). The GNPs on the fracture surface are well dispersed, with size of 2−5 μm, and no obvious agglomerates. It is difficult to break GNPs by stress due to their strong mechanical properties. The GNPs and the Al matrix can form a mechanically locked sum, which increases the difficulty of detaching the GNPs−Al interface. As a result, stress accumulates at the GNPs−Al interface when performing tensile tests. The stress leads to large deformation of the Al matrix, which appears as a large dimple after fracture. The load is also able to be transferred through the GNPs. The overall coordinated deformability of the Al matrix is enhanced by bridging GNPs, as shown in Fig. 11(c). The good bonding of the GNPs−Al interface is further proven by the load transfer through the GNPs.

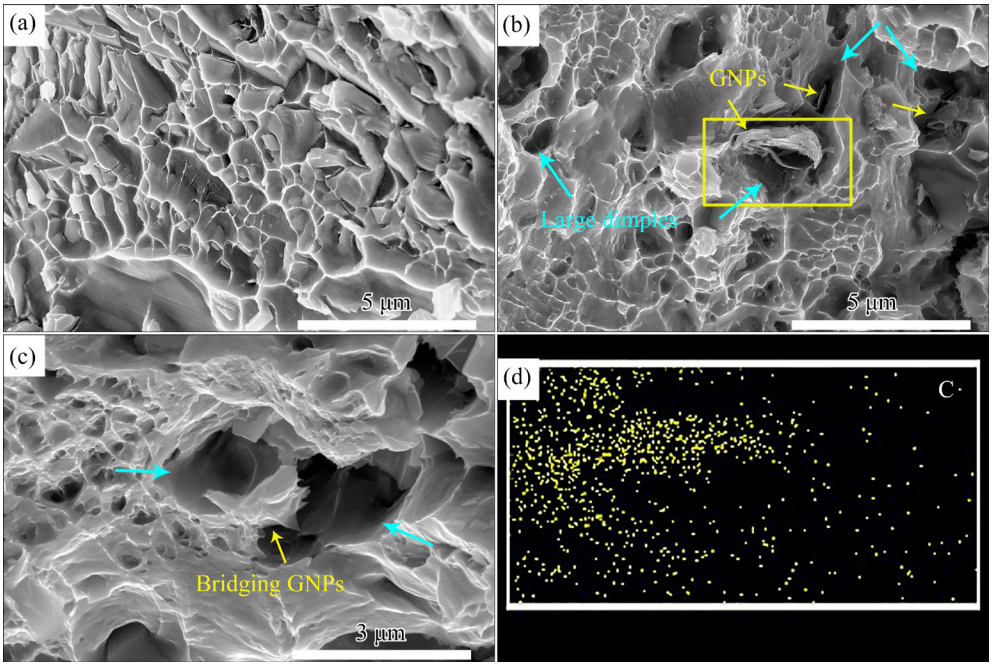

Fig. 11 Fracture morphology of peak-aged A380 alloy (a) and GNPs/A380 composites (b, c), and EDS results (d) for C element of rectangular area in (b)

4 Conclusions

(1) The addition of GNPs increases the dislocation density and GNPs−Al interface in the composites, which facilitates the reduction of the activation energy of Cu element, thus increasing the diffusion rate of Cu element.

(2) The CTE mismatch between GNPs and Al after solid solution treatment results in a large number of dislocations at the GNPs−Al interface. During aging treatment, dislocation annihilation and rearrangement allow the GNPs−Al interface to act as a more rapid and stable site for diffusion and nucleation of the precipitated phase.

(3) The yield strength of the GNPs/A380 composites increases by 28.1% after peak aging compared to the A380 alloy due to the fine grain strengthening, load transfer strengthening and precipitation strengthening resulting from the addition of GNPs. Due to bridging GNPs, the coordinated deformation of the matrix increases and larger dimples appear on the fracture surface of the GNPs/A380 composites.

CRediT authorship contribution statement

Zhao-wei HUANG: Writing – Original draft, Visualization, Testing, Investigation; **Xiao-bin LU:** Methodology; **Hong YAN:** Supervision, Conceptualization, Methodology, Writing − Review & editing.

Declaration of competing interest

The authors declare that they have no known competing financial interests or personal relationships that could have appeared to influence the work reported in this paper.

Data availability statement

Data will be made available on request.

Acknowledgments

This study was supported by the National Natural Science Foundation of China (No. 51965040).

References

[1] BASTWROS M, KIM Gap-yong, ZHU Can, ZHANG Kun, WANG Shi-ren, TANG Xiao-duan, WANG Xin-wei. Effect of ball milling on graphene reinforced Al6061 composite fabricated by semi-solid sintering [J]. Composites, Part B: Engineering, 2014, 60: 111−118. https://doi.org/10.1016/j.compositesb.2013.12.043.

[2] BALANDIN A A, GHOSH S, BAO Wen-zhong, CALIZO I, TEWELDEBRHAN D, MIAO Feng, LAU C N. Superior thermal conductivity of single-layer graphene [J]. Nano Letters, 2008, 8: 902−907. https://doi.org/10.1021/nl0731872.

[3] TJONG S C. Recent progress in the development and properties of novel metal matrix nanocomposites reinforced with carbon nanotubes and graphene nanosheets [J]. Materials Science and Engineering: R, 2013, 74: 281−350. https://doi.org/10.1016/j.mser.2013.08.001.

[4] ZHOU Wei-wei, YAMAGUCHI T, KIKUCHI K, NOMURA N, KAWASAKI A. Effectively enhanced load transfer by interfacial reactions in multi-walled carbon nanotube reinforced Al matrix composites [J]. Acta Materialia, 2017, 125: 369−376. https://doi.org/10.1016/j.actamat.2016.12.022.

[5] ALAM M A, YA H B, AZEEM M, MUSTAPHA M, YUSUF M, MASOOD F, MARODE R V, SAPUAN S M, ANSARI A H. Advancements in aluminum matrix composites reinforced with carbides and graphene: A comprehensive review [J]. Nanotechnology Reviews, 2023, 12: 20230111. https://doi.org/10.1515/ntrev-2023-0111.

[6] FENG Si-wen, GUO Qiang, LI Zan, FAN Gen-lian, LI Zhi-qiang, XIONG Ding-bang, SU Yi-shi, TAN Zhan-qiu, ZHAN Jie, ZHANG Di. Strengthening and toughening mechanisms in graphene−Al nanolaminated composite micro-pillars [J]. Acta Materialia, 2017, 125: 98−108. https://doi.org/10.1016/j.actamat.2016.11.043.

[7] ASGHARZADEH H, SEDIGH M. Synthesis and mechanical properties of Al matrix composites reinforced with few-layer graphene and graphene oxide [J]. Journal of Alloys and Compounds, 2017, 728: 47−62. https://doi.org/10.1016/j.jallcom. 2017.08.268.

[8] ALI A M, OMAR M Z, HASHIM H, SALLEH M S, MOHAMED I F. Recent development in graphene-reinforced aluminum matrix composite: A review [J]. Reviews on Advanced Materials Science, 2021, 60: 801−817. https://doi.org/10.1515/rams-2021-0062.

[9] ZHANG Hai-ping, XU Cong, XIAO Wen-long, AMEYAMA K, MA Chao-li. Enhanced mechanical properties of Al5083 alloy with graphene nanoplates prepared by ball milling and hot extrusion [J]. Materials Science and Engineering: A, 2016, 658: 8−15. https://doi.org/10. 1016/j.msea.2016.01.076.

[10] LIA Min, GAO Hai-yan, LIANG Jia-miao, GU Sun-wang, YOU We-ren, SHU Da, WANG Jun, SUN Bao-de. Microstructure evolution and properties of graphene nanoplatelets reinforced aluminum matrix composites [J]. Materials Characterization, 2018, 140: 172−178. https://doi.org/ 10. 1016/j.matchar.2018.04.007.

[11] YAN S J, DAI S L, ZHANG X Y, YANG C, HONG Q H, CHEN J Z, LIN Z M. Investigating aluminum alloy reinforced by graphene nanoflakes [J]. Materials Science and Engineering: A, 2014, 612: 440−444. https://doi.org/10.1016/j. msea.2014.06.077.

[12] SHIN S E, CHOI H J, SHIN J H, BAE D H. Strengthening behavior of few-layered graphene/aluminum composites [J]. Carbon, 2015, 82: 143−151. https://doi.org/10.1016/j.carbon.2014.10.044.

[13] ZHAO Mei, XIONG Ding-bang, TAN Zhan-qiu, FAN Gen-lian, GUO Qiang, GUO Cui-ping, LI Zhi-qiang,

ZHANG Di. Lateral size effect of graphene on mechanical properties of aluminum matrix nanolaminated composites [J]. Scripta Materialia, 2017, 139: 44−48. https://doi.org/10.1016/j. scriptamat.2017.06.018.

[14] SU Yi-shi, LI Zan, YU Yang, ZHAO Lei, LI Zhi-qiang, GUO Qiang, XIONG Ding-bang, ZHANG Di. Composite structural modeling and tensile mechanical behavior of graphene reinforced metal matrix composites [J]. Science China Materials, 2018, 61: 112−124. https://doi.org/10.1007/s40843-017-9142-2.

[15] YU Zhen-he, YANG Wen-shu, ZHOU Chang, ZHANG Ning-bo, CHAO Zhen-long, LIU Hao, CAO You-fang, SUN Yue, SHAO Pu-zhen, WU Gao-hui. Effect of ball milling time on graphene nanosheets reinforced Al6063 composite fabricated by pressure infiltration method [J]. Carbon, 2019, 141: 25−39. https://doi.org/10.1016/j.carbon.2018.09.041.

[16] LI D S, YE Y, LIAO X J, QIN Q H. A novel method for preparing and characterizing graphene nanoplatelets/aluminum nanocomposites [J]. Nano Research, 2018, 11: 1642−1650. https://doi.org/10.1007/s12274-017-1779-9.

[17] JIANG Yuan-yuan, TAN Zhan-qiu, FAN Gen-lian, WANG Lei, XIONG Ding-bang, GUO Qiang, SU Yi-shi, LI Zhi-qiang, ZHANG Di. Reaction-free interface promoting strength-ductility balance in graphene nanosheet/Al composites [J]. Carbon, 2020, 158: 449−455. https://doi.org/10.1016/j.carbon.2019.11.010.

[18] YU H, ZHANG S Q, XIA J H, SU Q, MA B C, WU J H, ZHOU J X, WANG X T, HU L X. Microstructural evolution, mechanical and physical properties of graphene reinforced aluminum composites fabricated via powder metallurgy [J]. Materials Science and Engineering: A, 2021, 802: 140669. doi.org/10.1016/j.msea.2020.140669.

[19] MOSTAFA K, MORTAZA A, MASUD E, MOHAMMAD A. Microstructure, hardness and tensile properties of A380 aluminum alloy with and without Li additions [J]. Materials Science and Engineering: A, 2013, 582: 409−414. https://doi.org/10.1016/j.msea.2013.05.088.

[20] QIU Xiang, WANG Ji-qiang, TARIQ N U H, GYANSAH L, ZHANG Jing-xuan, XIONG Tian-ying. Effect of heat treatment on microstructure and mechanical properties of A380 aluminum alloy deposited by cold spray [J]. Journal of Thermal Spray Technology, 2017, 26: 1898−1907. https://doi.org/10.1007/s11666-017-0640-8.

[21] ZHOU Xuan, GAO Yi-min, WANG Yi-ran, HUANG Xiao-yu, XIAO Peng. The improved strength and ductility of ZrC_p/2024Al composites with a quasi-network microstructure fabricated by spark plasma sintering and T6 heat treatment [J]. Materials Science and Engineering: A, 2022, 841: 142675. https://doi.org/10.1016/j.msea.2022.142675.

[22] YANG Hua-bing, GAO Tong, ZHANG Hua-ning, NIE Jin-feng, LIU Xiang-fa. Enhanced age-hardening behavior in Al−Cu alloys induced by in-situ synthesized TiC nanoparticles [J]. Journal of Materials Science & Technology, 2019, 35: 374−382. https://doi.org/10.1016/j.jmst.2018.09.029.

[23] CHEN Ma-lin, FAN Gen-lian, TAN Zhan-qiu, YUAN Chao, GUO Qiang, XIONG Ding-bang, CHEN Ming-liang, ZHENG Quan, LI Zhi-qiang, ZHANG Di. Heat treatment behavior and strengthening mechanisms of CNT/6061Al composites fabricated by flake powder metallurgy [J]. Materials Characterization, 2019, 153: 261−270. https://doi.org/10. 1016/j.matchar.2019.05.017.

[24] PAL S, MITRA R, BHANUPRASAD V V. Aging behaviour of Al−Cu−Mg alloy−SiC composites [J]. Materials Science and Engineering: A, 2008, 480: 496−505. https://doi:10.1016/j. msea.2007.07.072.

[25] AVAL H J. Effects of aging heat treatment on microstructure and corrosion behavior of friction surfacing treated Al−Zn−Mg−Cu matrix composite [J]. Transactions of Nonferrous Metals Society of China, 2023, 33: 2303−2313. https://doi:10.1016/S1003-6326(23)66260-0.

[26] FARAJOLLAHI R, AVAL H J, JAMAATI R. Non-isothermal aging behavior of in-situ AA2024−Al_3NiCu composite [J]. Transactions of Nonferrous Metals Society of China, 2022, 32: 2125−2137. https://doi:10.1016/S1003-6326(22) 65935-1.

[27] HUANG Zhao-wei, YAN Hong. Effect of graphene on the microstructure evolution and mechanical properties of Al−10Si−2Cu−1.5Fe aluminum matrix composites [J]. International Journal of Metalcasting, 2023, 17: 2808−2817. https://doi.org/10.1007/s40962-022-00952-0.

[28] WANG Meng, XU W, HAN Qing-you. Effect of heat treatment on controlling the morphology of AlFeSi phase in A380 alloy [J]. International Journal of Metalcasting, 2016, 10: 516−523. https://doi.org/10.1007/s40962-016-0068-9.

[29] RINGER S P, HONO K, POLMEAR I J, SAKURAI T. Nucleation of precipitates in aged Al−Cu−Mg−(Ag) alloys with high Cu: Mg ratios [J]. Acta Materialia, 1996, 44: 1883−1898.

[30] CAI Qing, MENDIS C L, WANG Shi-hao, CHANG I T H, FAN Zhong-yun. Effect of heat treatment on microstructure and tensile properties of die-cast Al−Cu−Si−Mg alloys [J]. Journal of Alloys and Compounds, 2021, 881: 160559. https://doi.org/10.1016/j.jallcom.2021.160559.

[31] LI Hui-zhong, ZHU Ze-xiao, LIANG Xiao-peng, LI Peng-wei, QI Ye-long, LV Feng, HUANG Lan. Effect of T6-treatments on microstructure and mechanical properties of forged Al−4.4Cu−0.7Mg−0.6Si alloy [J]. Transactions of Nonferrous Metals Society of China, 2017, 27: 2539−2547. https://doi.org/10.1016/S1003-6326(17)60282-6.

[32] CHEN Xiao-feng, QIAN Feng, BAI Xiang-ren, ZHAO Dong-dong, ZHANG Xiang, LI Jia-jun, HE Chun-nian, SHI Chun-shen, TAO Jing-mei, ZHAO Nai-qin. Formation of the orientation relationship-dependent interfacial carbide in Al matrix composite affected by architectured carbon nanotube [J]. Acta Materialia, 2022, 228: 117758. https://doi.org/10.1016/j.actamat.2022.117758.

[33] GOKCEN N A, ODEN L L. Phase equilibria in aluminum-carbon system at high temperatures [J]. Journal of Phase Equilibria, 1998, 19: 409.

[34] HUANG Zhao-wei, YAN Hong, XIONG Jun-jie. Analysis of microstructure and mechanical properties of graphene nanoplatelet reinforced 2024Al alloy [J]. Materials Science and Engineering: A, 2022, 832: 142466. https://doi.org/10.1016/j. msea.2021.142466.

[35] KIM K T, ECKERT J, MENZEL S B, GEMMING T, HONG S H. Grain refinement assisted strengthening of

carbon nanotube reinforced copper matrix nanocomposites [J]. Applied Physics Letters, 2008, 92: 121901. https://doi.org/10.1063/1.2899939.

[36] LI Jian-chao, ZHANG Xue-xi, GENG Lin. Effect of heat treatment on interfacial bonding and strengthening efficiency of graphene in GNP/Al composites [J]. Composites, Part A: Applied Science and Manufacturing, 2019, 121: 487−498. https://doi.org/10.1016/j.compositesa.2019.04.010.

[37] SHARMA A, MORISADA Y, FUJII H. Bending induced mechanical exfoliation of graphene interlayers in a through thickness Al-GNP functionally graded composite fabricated via novel single-step FSP approach [J]. Carbon, 2022, 186: 475−491. https://doi.org/10.1016/j.carbon.2021.10.018.

[38] KELLY A, TYSON W R. Tensile properties of fibre-reinforced metals: Copper/tungsten and copper/molybdenum [J]. Journal of the Mechanics and Physics of Solids, 1965, 13: 329−350. https://doi.org/10.1016/0022-5096(65)90035-9.

[39] GUO Bai-song, CHEN Yi-qiang, WANG Zhang-wei, YI Jian-hong, NI Song, DU Yong, LI Wei, SONG Min. Enhancement of strength and ductility by interfacial nano-decoration in carbon nanotube/aluminum matrix composites [J]. Carbon, 2020, 159: 201−212. https://doi.org/10.1016/j.carbon. 2019.12.038.

[40] BHADAURIA A, SINGH L K, L AHA T, Combined strengthening effect of nanocrystalline matrix and graphene nanoplatelet reinforcement on the mechanical properties of spark plasma sintered aluminum based nanocomposites [J]. Materials Science and Engineering: A, 2019, 749: 14−26. https://doi.org/10.1016/j.msea.2019.02.007.

[41] WANG X J, HU X S, LIU W Q, DU J F, WU K, HUANG Y D, ZHENG M Y. Ageing behavior of as-cast SiC_p/AZ91 Mg matrix composites [J]. Materials Science and Engineering: A, 2017, 682: 491−500. https://dx.doi.org/10.1016/j.msea. 2016.11.072.

[42] XIAO Peng, GAO Yi-min, YANG Xi-rong, XU Fei-xing, YANG Cui-cui, LI B, LI Ye-fei, LIU Zhi-wei, ZHENG Qiao-ling. Processing, microstructure and ageing behavior of in-situ submicron TiB_2 particles reinforced AZ91 Mg matrix composites [J]. Journal of Alloys and Compounds, 2018, 764: 96−106. https://dx.doi.org/10.1016/j.jallcom.2018.05.351.

[43] ZOU Xiu-liang, YAN Hong, CHEN Xiao-hui. Evolution of second phases and mechanical properties of 7075 Al alloy processed by solution heat treatment [J]. Transactions of Nonferrous Metals Society of China, 2017, 27: 2146−2155. https://doi.org/10.1016/S1003-6326(17)60240-1.

[44] PATIL A, KIRAN Y N M S, OZDEMIR F, BANERJEE R, GUPTA R K, BORKARO T. Enhancement of the mechanical properties of graphene nanoplatelet (GNP) reinforced nickel matrix nanocomposites [J]. Materials Science and Engineering: A, 2021, 817: 141324. https://doi.org/ 10.1016/j.msea.2021.141324.

[45] YU Wei, WANG Yin, LI Yong, QIAN Xiao-ming, WANG Hai-yao, ZHOU Chien, WANG Zhao-dong, XU Guang-ming. Texture evolution, segregation behavior, and mechanical properties of 2060 Al-Li (aluminium-lithium) composites reinforced by TiC (titanium carbide) nanoparticles [J]. Composites, Part B: Engineering, 2023, 255: 110611. https://doi.org/10.1016/j.compositesb.2023. 110611.

[46] LI Min, ZHANG Zhen, GAO Hai-yan, WANG Yu-fei, LIANG Jia-miao, SHU Da, WANG Jun, SUN Bao-de. Formation of multilayer interfaces and the load transfer in graphene nanoplatelets reinforced Al matrix composites [J]. Materials Characterization, 2020, 159: 110018. https://doi.org/10. 1016/j.matchar.2019.110018.

[47] XU Jie, SUN Tong, XU Yan-tao, HAN Qing-hua. Fracture toughness research of G20Mn5QT cast steel based on the acoustic emission technique [J]. Construction and Building Materials, 2020, 230: 116904. https://doi.org/10.1016/j. conbuildmat.2019.116904.

石墨烯纳米片增强 A380 复合材料的时效行为、显微组织和力学性能

黄兆威[1,2]，卢晓斌[3]，闫 洪[1,2]

1. 南昌大学 先进制造学院，南昌 330031；
2. 南昌市轻合金制备与加工重点实验室，南昌 330031；
3. 高安市璐克斯机械有限公司，高安 330800

摘 要：采用超声波振动铸造法制备石墨烯纳米片(GNPs)增强 A380 复合材料(GNPs/A380 复合材料)。研究复合材料的显微组织、时效行为和力学性能。研究发现，GNPs 可缩短 GNPs/A380 复合材料的峰值时效时间，GNPs−Al 界面可作为析出相更稳定的成核点。通过 GNPs 的桥接，基体的协调变形增加，GNPs/A380 复合材料的断裂面上出现更大韧窝。由于细晶粒强化、载荷传递和沉淀强化机制，GNPs/A380 复合材料的屈服强度比 A380 合金提高了 28.1%。

关键词：石墨烯纳米片；铝基复合材料；时效处理；显微组织；力学性能

(Edited by Xiang-qun LI)